Enhanced photoacoustic microscopy with physics-embedded degeneration learning

Haigang Ma[1,2,3]*, Shili Ren[1,2,3], Xiang Wei[1,2,3], Yinshi Yu[1,2,3], Jiaming Qian[1,2,3], Qian Chen[1,3]* and Chao Zuo[1,2,3]*

[1]Smart Computational Imaging Laboratory (SCILab), School of Electronic and Optical Engineering, Nanjing University of Science and Technology, Nanjing 210094, China; [2]Smart Computational Imaging Research Institute (SCIRI) of Nanjing University of Science and Technology, Nanjing 210019, China; [3]Jiangsu Key Laboratory of Spectral Imaging & Intelligent Sense, Nanjing 210094, China.
*Correspondence: HG Ma, E-mail: mahaigang@njust.edu.cn; Q Chen, E-mail: chenqian@njust.edu.cn; C Zuo, E-mail: zuochao@njust.edu.cn

This file includes:

Supplementary information for this paper is available at https://doi.org/10.29026/oea.2025.240189

Section 1: Discussion on using different methods for simulation data

In the main content, our method can achieve noise reduction and resolution improvement at various levels. Here, the following will compare and analyze different methods and our methods. First of all, the following will analyze the denoising ability of three methods (cGAN, U-Net, ours). As shown in Fig. S1(a–e), our method outperforms other methods in SSIM and PSNR, effectively recovering signals masked by noise. In Fig. S1(f–j), a resolution quantification analysis is primarily conducted, but there is also some interference from noise and signal attenuation. The results show that our method outperforms other methods in terms of SSIM and PSNR. In Fig. S1(i), some large vessels are enhanced, which may be due to the U-net architecture misclassifying large vessels as small vessel structures.
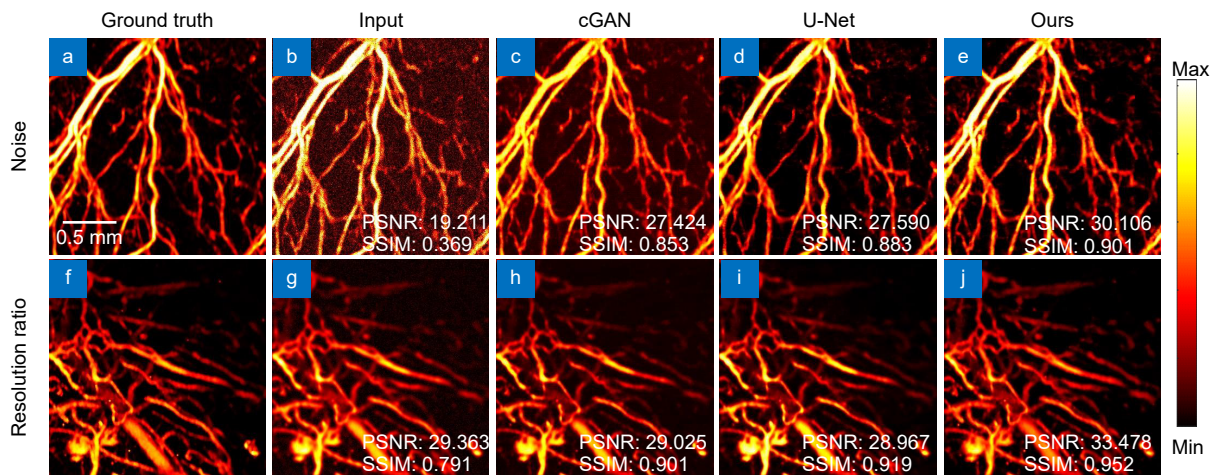
Fig. S1 | Comparison of cGAN, U-NET and ours methods. (**a–e**) Quantitative analysis of denoising by three methods. (**a**) Ground truth photoacoustic microscopy image. (**b**) Input photoacoustic microscopy image. (**c**) Photoacoustic microscopy image reconstructed from (b). (**d**) Photoacoustic microscopy image reconstructed from (b). (**e**) Image reconstructed from (b). (**f–j**) Quantitative analysis of resolution enhancement by three methods. (**f**) Ground truth photoacoustic microscopy image. (**g**) Input photoacoustic microscopy image. (**h**) Photoacoustic microscopy image reconstructed from (**g**). (**i**) Photoacoustic microscopy image reconstructed from (**g**). (**j**) Image reconstructed from (**g**).

Section 2: Supplement of experimental data at different depths

In the experiment of simulating photoacoustic microscopy imaging at different depths using translucent silicone of varying thicknesses, it is difficult to discern resolution and denoising effects due to the use of uniform color scales. As shown in Fig. S2, different color scales are used to better illustrate resolution and noise removal. After changing the color scale, it is evident that as thickness increases, image resolution and noise increase. Fig. S2(a_1–a_2) show that our method significantly improves resolution and denoising. With one silicone layer, the improvement in FWHM is not obvious, but as thickness increases, changes in FWHM become apparent. This is because the improvement in FWHM cannot exceed the actual thickness of the vessels. The adaptation of PEDL can be well reflected here.
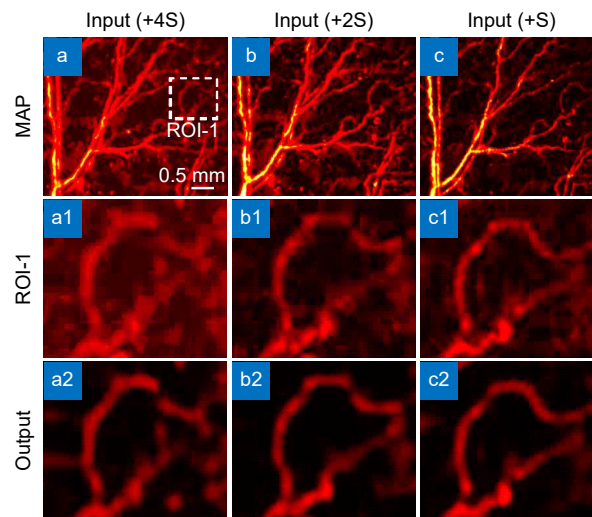
Fig. S2 | Comparison of results at different depths. (**a**) Photoacoustic microscopy image with four layers of silicone sheets. (**b**) Photoacoustic microscopy image with two layers of silicone sheets. (**c**) Photoacoustic microscopy image with one layer of silicone sheet. (**a1**–**a2**) Enlarged image and reconstructed image using our method with four layers of silicone sheets. (**b1**–**b2**) Enlarged image and reconstructed image using our method with two layers of silicone sheets. (**c1**–**c2**) Enlarged image and reconstructed image using our method with one layer of silicone sheet.

Section 3: Supplementary experimental data about denoising

In the experiments of this work, the noise in the acquired experimental data is not significant enough to demonstrate the denoising capability of our method. Adjusting the averaging of signals can increase noise; reducing the number of scans or skipping averaging retains more noise, significantly lowering the image SNR. When the motor overheats, additional noise is generated, interfering with the PAM system and further reducing the image SNR. Increasing the motor's workload can simulate this high-noise environment. Additionally, by adjusting the denoising ability of the equipment, such as modifying the denoising algorithm parameters or reducing filtering intensity, more noise components are retained in the image, effectively enhancing noise levels. These methods collectively provide high-noise photoacoustic microscopy image data, which are then processed using the denoising method proposed in this work. The specific experimental images are shown in Fig. S3. In Fig. 3, it is evident that our method effectively removes noise and retains signals masked by noise, as shown from Fig. S3(a) to Fig. S3(d). The white spots in Fig. S3(b) are due to excessive energy, but our method can still effectively remove these noises.
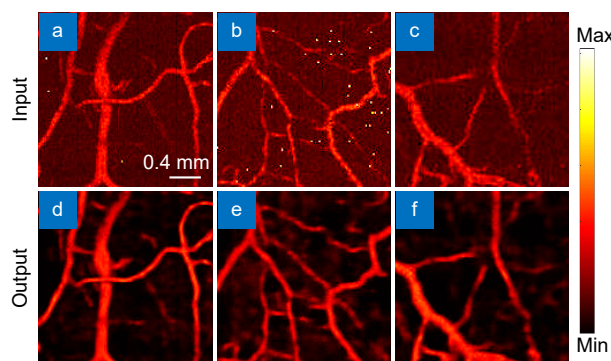
Fig. S3 | Denoising of real noisy images. (**a**–**c**) Photoacoustic microscopy images of different regions of a mouse ear. (**d**–**f**) Reconstructed images of (a–c) using our method.

Section 4: Supplementary data on mouse brain

In the experiments of this study, the mouse brain data obtained cannot definitively confirm that the reconstructed vasculature corresponds to actual existing structures. Therefore, partial vascular structures from the mouse brain are used as input, with PEDL applied for reconstruction. A thresholding algorithm is employed to highlight image pixels with intensities above a certain value. As shown in Fig. S4, the vascular signals reconstructed by PEDL can be observed in the
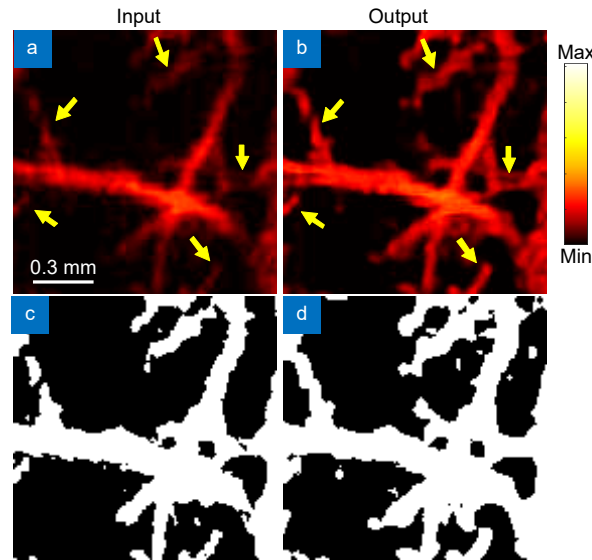
Fig. S4 | Image analysis of small area of mouse brain. (**a**) Input image of mouse brain. (**b**) Image of mouse brain reconstructed by PEDL. (**c**) Threshold image of mouse brain input image. (**d**) PEDL reconstructs the threshold image of mouse brain image.

thresholded input image in the region marked by the yellow arrows. However, due to the low intensity in the input image, these signals are difficult to characterize effectively. After reconstruction with PEDL, the vascular structures are significantly enhanced and successfully restored.

Section 5: Parameter definition

To avoid confusion caused by different calculation formulas, the specific formulas for CNR and SNR are provided below:

$$CNR = 40\frac{abs(\mu_{t} - \mu_{b})}{\delta_{b}} \, , \tag{S1}$$

$$SNR = 15\frac{Mean_{s}}{\delta_{n}} \, , \tag{S2}$$

where, μ_{t} represents the mean value of the target region. μ_{b} represents the mean value of the background region. δ_{b} represents the standard deviation calculated from the sum of variances of the target and background regions. $Mean_{s}$ represents the mean value of the image signal. δ_{n} represents the standard deviation of the noise. The constants 40 in the CNR formula and 15 in the SNR formula are commonly used scaling factors to adjust the results to an appropriate range, making them more suitable for experimental requirements and interpretation.